A Resonance Raman Investigation of Myoglobin and Hemoglobin

O. Bangcharoenpaurpong, K. T. Schomacker, and P. M. Champion*†

Contribution from the Department of Chemistry, Worcester Polytechnic Institute, Worcester, Massachusetts 01609. *Received February 8, 1984*

Abstract: We have measured the Raman excitation profiles (REP's) of some of the key vibrational modes of deoxy Mb and deoxy Hb. Use of new theoretical techniques that are based on the optical theorem and Kramers–Kronig relations allows us to directly measure the linear Franck–Condon coupling strengths of these modes. We also demonstrate how these theoretical techniques can lead to the "deconvolution" of overlapping diffuse electronic transitions by REP measurements of vibrational modes that couple independently to the transitions of interest. In addition, the effects of inhomogeneous (conformational) broadening are briefly explored. It is found that conformational broadening will express itself in subtle variations of the REP line shape for the high-frequency modes and in Raman scattering intensity variations for the low-frequency modes. These effects are discussed in the context of the Mb and Hb data. In the case of the important Fe–N_{His} vibration at ca. 220 cm^{-1}, we find that it is relatively strongly coupled ($S \simeq 0.06$–0.16) to the Soret transition and *not* to a separate blue-shifted charge-transfer transition. The feature at ca. 150 cm^{-1}, on the other hand, appears to have a distinct blue shift in its REP for which we do not have a satisfactory explanation. Finally, we present a new hypothesis that qualitatively explains the relatively strong coupling of the Fe–N_{His} mode to the Soret resonance as well as numerous other Raman and thermodynamic observations that relate to the phenomenon of Hb cooperativity.

I. Introduction

Myoglobin (Mb) and hemoglobin (Hb) are without doubt the two most widely studied heme proteins. The investigation of the molecular mechanisms of oxygen binding, storage, and release in these systems has involved the efforts of a wide range of scientists and a variety of physical, chemical, and biochemical techniques for many years. Nevertheless, many questions still remain unanswered, particularly regarding the detailed electronic and nuclear structure–function relationships controlling the oxygen–protein interaction.

During the last few years, resonance Raman spectroscopy has yielded significant information about the active site structure of a variety of heme proteins including Hb and Mb.[1] One of the main reasons for its success is due to the selective nature of the probe, namely, the resonance enhancement of the scattering cross sections of only those normal modes of the system that are "coupled" to the resonant electronic excitation. The coupling is selective due to the fact that (for visible and near-ultraviolet laser frequencies) the electronic excitation is more or less "localized" on the heme ring and/or on the iron–axial ligand bonds. As a result of this selective coupling, the inelastic light scattering due to vibrations of the heme chromophore as well as the axial ligands are often observed well above the background scattering due to the numerous other vibrational modes of these macromolecular systems. Such selectivity results in greatly simplified spectra and allows a reasonable chance for the assignment of mode frequencies by isotopic labeling or comparative studies.

Recently, work on the Mb and Hb problem with use of resonance Raman spectroscopy has enjoyed significant progress. The assignment of the Fe–N(histidine) mode at ca. 216–220 cm^{-1} by Kitagawa and co-workers[2,3] has led to a variety of investigations involving R → T conformational changes[3,4] as well as histidine deprotonation,[5,6] cryogenic,[7-10] and comparative[11] studies. The identification of the iron–oxygen stretching vibration in Hb[12] at ca. 570 cm^{-1} as well as the O–O vibration in cobalt-substituted Hb and Mb[13] at 1135 cm^{-1} has resulted in further Raman studies[6,14] that may ultimately help to elucidate the detailed mechanism of action of these proteins. Additional work involving iron–ligand vibrations of the met[15] and carbon monoxide[16] forms of Hb and Mb has also led to interesting implications regarding the electronic and nuclear structure of the active site.

In the present work we explore in detail the resonance enhancement of some of the key Raman vibrational frequencies of deoxy Mb, Hb, and met Mb. In particular, recent theoretical advances in our understanding of resonance Raman scattering in the multimode limit[17] are brought to bear on the Hb and Mb problem. These advances exploit the Kramers–Kronig relationship between the absorption and resonance-scattering cross sections and have come to be called the transform theory.[18-22] One important point that is not yet widely recognized is the fact that electron–nuclear coupling strengths can be found *directly*,[21-24] without the use of additional modeling parameters, once the resonance Raman scattering intensity (i.e., cross section) is measured on an absolute scale. Use of the transform method to analyze the position of the Raman Excitation Profile (REP) and its line shape with respect to the absorption band also gives important information regarding the electronic transitions and the type of coupling mechanisms responsible for the resonance enhancement.

Surprisingly, we find a coupling strength for the Fe–N_{His} vibration of Mb that is many times larger than other heme vibrational modes coupled to the π–π^* transitions of the heme group. As will be shown below, detailed analysis of the REP line shape, position, and intensity as well as the lack of strong overtone

† Present address: Department of Physics, Northeastern University, Boston, Massachusetts 02115.

(1) Spiro, T. G. In "Iron Porphyrins"; Part II; Lever, A., Grey, H., Eds.; Addision-Wesley: Reading, 1983; p 89.
(2) Kitagawa, T.; Nagai, K.; Tsubaki, M. *FEBS Lett.* **1979**, *104*, 376.
(3) Nagai, K.; Kitagawa, T.; Morimoto, H. *J. Mol. Biol.* **1980**, *136*, 271.
(4) Nagai, K.; Kitagawa, T. *Proc. Natl. Acad. Sci. U.S.A.* **1980**, *77*, 2033.
(5) Stein, P.; Mitchell, M.; Spiro, T. *J. Am. Chem. Soc.* **1980**, *102*, 7795.
(6) Walters, M.; Spiro, T. *Biochemistry* **1982**, *21*, 6989.
(7) Ondrais, M.; Rousseau, D.; Simon, S. *Science* **1981**, *213*, 657.
(8) Ondrais, M.; Rousseau, D.; Simon, S. *Proc. Natl. Acad. Sci. U.S.A.* **1982**, *79*, 1511.
(9) Ondrais, M.; Friedman, J.; Rousseau, D. *Science* **1983**, *220*, 615.
(10) Ondrais, M.; Rousseau, D.; Simon, S. *J. Biol. Chem.* **1983**, *258*, 5638.
(11) Irwin, M.; Armstrong, R.; Wright, P. *FEBS Lett.* **1981**, *133*, 239.
(12) Brunner, H. *Naturwissenschaften* **1974**, *61*, 129.
(13) Tsubaki, M.; Yu, N. T. *Proc. Natl. Acad. Sci. U.S.A.* **1981**, *78*, 3851.
(14) Kitagawa, T.; Ondrais, M.; Rousseau, D.; Ikeda-Saito, M.; Yonetani, T. *Nature (London)* **1982**, *298*, 869.
(15) Asher, S.; Schuster, T. *Biochemistry* **1979**, *18*, 5377.
(16) Tsubaki, M.; Srivastava, R.; Yu, N. T. *Biochemistry* **1982**, *21*, 1131.
(17) Champion, P. M.; Albrecht, A. C. *Annu. Rev. Phys. Chem.* **1982**, *33*, 353.
(18) Hizhnyakov, V.; Tehver, I. *Phys. Status Solidi* **1967**, *21*, 755.
(19) Tonks, D. L.; Page, J. B. *Chem. Phys. Lett.* **1979**, *66*, 449.
(20) Hassing, S.; Mortensen, O. S. *J. Chem. Phys.* **1980**, *73*, 1078.
(21) Champion, P. M.; Albrecht, A. C. *Chem. Phys. Lett.* **1981**, *82*, 410.
(22) Stallard, B.; Champion, P. M.; Callis, P. R.; Albrecht, A. C. *J. Chem. Phys.* **1983**, *78*, 712.
(23) Stallard, B.; Callis, P. R.; Champion, P. M.; Albrecht, A. C. *J. Chem. Phys.* **1984**, *80*, 70.
(24) Schomacker, K.; Bangcharoenpaurpong, O.; Champion, P. M. *J. Chem. Phys.* **1984**, *80*, 4701.

0002-7863/84/1506-5688$01.50/0

scattering have convinced us that the Fe–N_{His} mode is coupled to the Soret band π–π^* resonance and *not* to a separate charge-transfer band. Ironically, this study was undertaken with the hope of finding and characterizing a charge-transfer resonance buried to the blue of the Soret maximum as speculated by Ondrais et al.[10] and suggested by the data of Irwin et al.[11] Nevertheless, the data we have obtained imply a previously unsuspected degree of electronic interaction between the histidine, iron, and porphyrin orbitals. For example, it follows directly from our observations that the level of electron density in the π^* orbitals of the porphyrin must significantly affect the potential energy surface and equilibrium position of the Fe–N_{His} bond. It appears that one type of interaction consistent with the observed magnitude of the coupling strength involves direct π^*_{por}–$\sigma^*_{Fe-N_{His}}$ ("dz^2") overlap. Such interactions conceivably play an important role in the phenomenon of oxygen binding and Hb cooperativity since the partially filled $\sigma^*_{Fe-N_{His}}$ orbital is involved in the bonding of molecular oxygen.

In addition to the experimental results, we also briefly explore, theoretically, the effects of ensemble averaging that lead to inhomogeneous broadening of the absorption band and REP line shape. It is found that such effects show dispersion with the frequency of the Raman mode under study. The previously discussed[22,24] dispersion of coupling strength with Raman frequency is also presented explicitly for deoxymyoglobin in order to help explain why such a large coupling strength is found for the low-frequency 220-cm^{-1} mode without the intuitively expected large increase in Raman scattering intensity. Finally, we demonstrate, using synthetic spectra, a technique for the deconvolution of absorption bands using the concept of the inverse transform.[21,25] We wish to emphasize that if the REP's are measured on the absolute cross-section scale, the coupling strengths as well as extinction coefficients of individual transitions can be obtained even under the more complex conditions of overlapping electronic absorption spectra.

II. Theory

The transform theory has been discussed in great detail elsewhere,[19-28] so we will not burden the reader with a lengthy presentation. Instead, we will outline some of the key ideas and demonstrate the process by which coupling strengths can be extracted from the data by the simultaneous analysis of Raman and absorption spectra. In addition, we will give a brief operational procedure for the deconvolution of overlapping absorption bands using inverse transform techniques.[21,25] Finally, we will critically explore, via theoretical computer simulation, the effects of inhomogeneous broadening (i.e., site broadening) on calculations of the coupling strengths.

A. Transform. For simplicity in presentation, we confine ourselves to the linear coupling of harmonic potential energy surfaces (Condon approximation) as shown in Figure 1. Such coupling (commonly known as *A* term[29]) gives rise to resonance Raman scattering of totally symmetric modes and is the dominant scattering mechanism in strongly allowed transitions such as the Soret region of heme proteins. Non-Condon vibronic coupling between two or more excited states (*B* term) or the ground state (*C* term) can also be an active mechanism for the Raman scattering of totally symmetric modes. As we have shown in previous studies,[22,23] such coupling can be incorporated into the transform theory even at the non-adiabatic level.[30] However, these previous studies find that only a small non-Condon contribution is necessary (~2% at intensity level) in order to achieve an essentially perfect fit to the REP line shape of the 1362-cm^{-1} mode of cytochrome *c*. Such fitting procedures allow crude estimates of the off-diagonal (non-Condon) vibronic matrix elements to be made.[23] On the other hand, the Condon scattering is governed by the diagonal coupling elements, given by $\bar{\nu}_R S^{1/2}$ (see Figure 1), which are found quite accurately by using the transform theory to fit the absolute intensity as well as the shape of the REP.

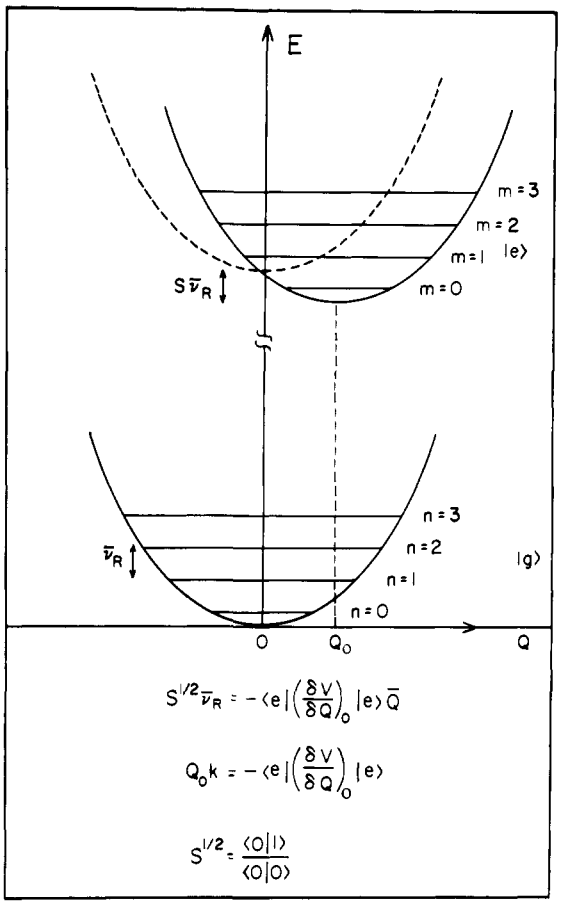

Figure 1. The standard model of linear harmonic coupling used in this work. The shift of the nuclear potential energy surface in the excited state ($|e\rangle$) is completely specified by *S*, the coupling strength. The quantity $\bar{\nu}_R$ is the frequency of the Raman mode under consideration. Note that only this mode needs to be factored from the molecular eigenstate in the Born–Oppenheimer approximation.[22] The Stokes shift along the energy axis of the excited-state surface is given by $S\bar{\nu}_R$. The quantity $\bar{Q}$ is the root-mean-square zero-point displacement of the Raman mode.

A variety of recent efforts at understanding the detailed nature of Raman excitation profiles in heme proteins have involved multiparameter fitting procedures[31-33] that have focused almost exclusively on the shapes of the profiles or on the relative intensities of the scattering between the Q and B bands.[34,35] As a result of ambiguities in the multiparameter set that best generates the shape of an experimental REP, we feel that such approaches are inherently limited in their effectiveness. For example, as discussed recently,[24] the non-adiabatic correction to the (*A* term) Condon approximation cannot be formally separated from the non-Condon corrections (e.g., *B*, *C* term interference) unless anti-Stokes REP's are also monitored. Our original work in this area[31] also employed a multiparameter fitting procedure that was later shown[21] to be an exact representation of the transform theory in the Condon approximation. The explicit exposure of the coupling strength in the original theory was not made, however, and no fits to the absolute scattering intensity were attempted. Such an approach focuses attention on the asymmetries found in both the absorption and REP line shapes rather than on the absolute intensity which

(25) Lee, D.; Stallard, B.; Champion, P. M.; Albrecht, A. C. *J. Phys. Chem.*, in press.
(26) Tonks, D.; Page, J. B. *Chem. Phys. Lett.* **1981**, *79*, 247.
(27) Tonks, D.; Page, J. B. *J. Chem. Phys.* **1982**, *76*, 5820.
(28) (a) Page, J. B.; Tonks, D. L. *J. Chem. Phys.* **1981**, *75*, 5694. (b) Chan, C. K.; Page, J. B. *J. Chem. Phys.* **1984**, *79*, 5234.
(29) Tang, J.; Albrecht, A. C. In "Raman Spectroscopy"; Szymanski, H., Ed.; Plenum: New York, 1970; p 33.
(30) Small, G. J.; Yeung, E. S. *Chem. Phys.* **1975**, *9*, 379.
(31) Champion, P. M.; Albrecht, A. C. *J. Chem. Phys.* **1979**, *71*, 1110.
(32) Shelnutt, J. J. *Chem. Phys.* **1981**, *74*, 6644.
(33) Siebrand, W.; Zgierski, M. *Chem. Phys.* **1983**, *77*, 35.
(34) Shelnutt, J. *J. Chem. Phys.* **1980**, *72*, 3948.
(35) Champion, P. M.; Albrecht, A. C. *J. Chem. Phys.* **1981**, *75*, 3211.

can directly provide the linear Franck–Condon coupling strength. Since in this work we are stressing the latter concept, we hold strictly to the Condon approximation and write for the Stokes scattering of fundamentals:[24,28b]

$$R_T(\bar{\nu}) = (\text{constant})(\bar{\nu} - \bar{\nu}_a)^3\bar{\nu}(\langle n\rangle + 1)S_a|\alpha_T(\bar{\nu})|^2 \quad (1)$$

where

$$R_T(\bar{\nu}) = \left(\frac{d\sigma}{d\Omega}\right)_{\parallel} - \frac{4}{3}\left(\frac{d\sigma}{d\Omega}\right)_{\perp} = \frac{3 - 4\rho}{3 + 3\rho}\left(\frac{d\sigma}{d\Omega}\right)_T \quad (2)$$

is the Raman invariant[20,22] for the scattering of totally symmetric modes at laser frequency $\bar{\nu}$. The $\langle n\rangle + 1$ factor is given by $[1 - e^{-\bar{\nu}_a/kT}]^{-1}$ and results from the thermal average over initial states of the system.[24,28] (The general applicability of eq 1 at finite temperature has been discussed by Chan and Page[28b] using time correlator techniques and by Schomacker et al.[24] using frequency domain expressions.) The depolarization ratio, ρ, is defined in eq 2 as usual by the ratio of the perpendicular polarized scattering cross section, $(d\sigma/d\Omega)_{\perp}$, to the parallel polarized scattering cross section, $(d\sigma/d\Omega)_{\parallel}$. The total cross section, $(d\sigma/d\Omega)_T$, is given by their sum. The coupling strength, S_a, is associated with the mode having a Raman shift, $\bar{\nu}_a$. The constant that scales eq 1 to the absolute Raman cross-section level is given by constant $= n_m{}^2 3.654 \times 10^{-42}$ when the absorption cross section at temperature T is recorded in the usual chemical units (i.e., molar decadic extinction coefficient, $\epsilon_T(\bar{\nu})$ (M^{-1} cm^{-1})). The quantity n_m is the index of refraction of the solvent medium. The complex function, $\alpha_T(\bar{\nu})$, is related by a constant to the resonant part of the molecular polarizability and is given by:

$$\alpha_T(\bar{\nu}) = \phi_T(\bar{\nu}) - \phi_T(\bar{\nu} - \bar{\nu}_a) \quad (3)$$

with

$$\phi_T(\bar{\nu}) = \frac{1}{\pi}\int_{-\infty}^{\infty}\frac{\epsilon_T(x)}{x(x - \bar{\nu})}\,dx + i\frac{\epsilon_T(\bar{\nu})}{\bar{\nu}} \quad (4)$$

Equation 4 can be seen to be a simple Kramers–Kronig transform that arises in a variety of physical problems and is used to fix the real part of the susceptibility once the imaginary part (i.e., the absorptivity) is known. (A similar approach is used, for example, in the analysis of the far-infrared magnetic resonance spectra of Hb and Mb[36]). The displacement function of eq 3 and the coupling strength in eq 1 both arise from use of the harmonic oscillator recursion relations in the Condon limit.[19–22]

It should be emphasized that eq 1–4 result from a single molecule theory and, as a result, are simplified versions of the more general equations that formally recognize inhomogeneous ensemble effects.[22,24] We will explore such effects and their dependence on Raman frequency momentarily. More generally, we want to stress the fact that eq 1–4 have only one free parameter (S_a) which can be found by simultaneously matching the observed resonant absorption and absolute Raman scattering cross sections.

If, on the other hand, the resonant absorption cross section is not obviously available (e.g., a buried charge-transfer transition with unknown extinction coefficient), we must recognize that additional steps are needed in the analysis of the data. The deconvolution of such overlapping absorption spectra by use of the inverse transform is the topic of the next section.

B. Inverse Transform. The concept of the inverse transform has been previously discussed,[21,37] and an efficient method for calculation has been presented.[25] What we wish to do here is to demonstrate how the deconvolution of two resonantly active absorption bands can effectively be carried out with eq 1–4 so that the extinction coefficients of *both* transitions as well as the coupling strengths of the active Raman modes can be determined.

As mentioned earlier, our initial motivation for the present experimental studies was the characterization and deconvolution of a suspected iron–histidine charge-transfer band lying to the blue of the Soret transition.[10,11] As will be seen in section IV, such a separate charge-transfer transition turns out *not* to be present in Mb and Hb. Nevertheless, we proceed in this section using model calculations in order to demonstrate, in principle, how one can use the transform theory to handle such situations, should they arise in other circumstances.

Let us assume that an out-of-plane iron–ligand charge-transfer transition having an extinction coefficient $\epsilon_{CT}(\bar{\nu})$ is buried to the blue of the intense π–π^* Soret transition, $\epsilon_\pi(\bar{\nu})$. In addition, we assume that a Raman-active iron–ligand mode, enhanced by $\epsilon_{CT}(\bar{\nu})$, is definitely identified (by isotopic labeling, for example). Similarly, we assume that a Condon active porphyrin mode coupled to the π–π^* transition is also observed.

We consider our experimental observables to be both the REP of the ligand mode, $R_{CT}(\bar{\nu})$, and the REP of the porphyrin mode, $R_\pi(\bar{\nu})$, accurately measured on an absolute cross-section scale. The additional experimental observable is the total absorption cross section which we write as:

$$\epsilon(\bar{\nu}) = \epsilon_\pi(\bar{\nu}) + \epsilon_{CT}(\bar{\nu}) \quad (5a)$$

or

$$\frac{\epsilon^m}{A^m}A(\bar{\nu}) = \frac{\epsilon^m{}_\pi}{A^m{}_\pi}A_\pi(\bar{\nu}) + \frac{\epsilon^m{}_{CT}}{A^m{}_{CT}}A_{CT}(\bar{\nu}) \quad (5b)$$

where $A(\bar{\nu})$, $A_\pi(\bar{\nu})$, and $A_{CT}(\bar{\nu})$ are the absorption band shapes for the total, π–π^*, and charge-transfer transitions, respectively (all normalized to unit area). The ϵ^m, A^m terms refer to the maximum values of the respective line shapes.

Use of the inverse transform technique discussed previously[21,25] allows us to find

$$A_\pi(\bar{\nu}) = \tau^{-1}[R_\pi(\bar{\nu})] \quad (6a)$$

and

$$A_{CT}(\bar{\nu}) = \tau^{-1}[R_{CT}(\bar{\nu})] \quad (6b)$$

from the observed REP's of the iron–ligand and the porphyrin modes. The details of the inverse transform, symbolically represented by $\tau^{-1}[\ ]$ in eq 6, have already been discussed[25] and will not be further elaborated here. It is interesting to note, however, that our original closed-form analysis[21,31] of absorption and REP line shapes is a particularly convenient route to finding the absorption line shape associated with a given REP[38] (or vice versa).

Once $A_{CT}(\bar{\nu})$ and $A_\pi(\bar{\nu})$ have been found from the experimental REP's, we simply find the weighting factor, Z, that most accurately produces the total absorption band shape (through least-squares analysis for example), i.e.

$$A(\bar{\nu}) = \frac{A_\pi(\bar{\nu}) + ZA_{CT}(\bar{\nu})}{1 + Z} \quad (7)$$

Having found Z, the deconvoluted extinction coefficients are given by:

$$\epsilon_\pi(\bar{\nu}) = \frac{\epsilon^m A_\pi(\bar{\nu})}{A^m(1 + Z)} = \frac{\epsilon^m\tau^{-1}[R_\pi(\bar{\nu})]}{A^m(1 + Z)} \quad (8a)$$

$$\epsilon_{CT}(\bar{\nu}) = \frac{\epsilon^m Z}{A^m(1 + Z)}A_{CT}(\bar{\nu}) = \frac{\epsilon^m Z\tau^{-1}[R_{CT}(\bar{\nu})]}{A^m(1 + Z)} \quad (8b)$$

The coupling strengths of interest then follow by scaling according to eq 1–4.

As a simple illustration of this technique, we display in Figure 2, left, the hypothetical REP's of a porphyrin ring breathing mode at 1357 cm^{-1} (triangles) and an iron–axial ligand vibration at 220 cm^{-1} (squares) which has its maximum shifted significantly to the blue (as would be expected for a charge-transfer band buried to the blue of the Soret transition). The third profile in Figure 2, left (circles), represents scattering from a low-frequency porphyrin mode at 370 cm^{-1} that is coupled to the π–π^* resonance.

(36) Champion, P. M.; Sievers, A. J. *J. Chem. Phys.* **1980**, *72*, 1569.
(37) Champion, P. M.; Stallard, B. R.; Wagner, G. C.; Gunsalus, I. C. *J. Am. Chem. Soc.* **1982**, *104*, 5469.

(38) The only criterion is that the fitting parameters allow enough flexibility to precisely match the observed REP.

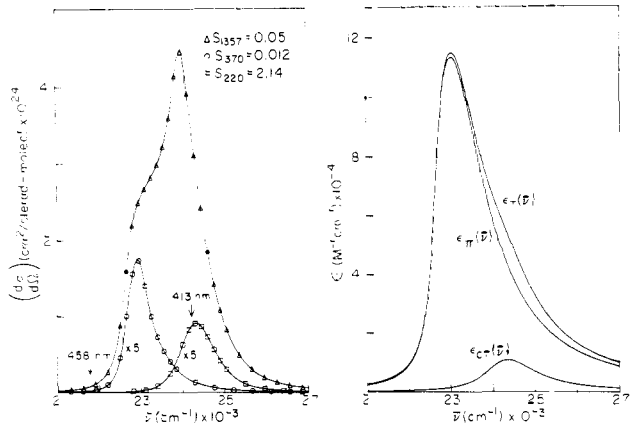

Figure 2. A simulation of a charge-transfer transition blue shifted from the Soret maximum. The 220-cm^{-1} mode is assumed to be coupled to this transition. The REP of the 220-cm^{-1} mode (squares) is inverse transformed to yield $A_{CT}(\bar{\nu})$. The REP of the 1357-cm^{-1} mode (triangles) is inverse transformed to yield $A_\pi(\bar{\nu})$. The REP of the 370-cm^{-1} mode (circles) is given in order to demonstrate the expected profile of a low-frequency mode coupled to the Soret band. Note the relative enhancement of the 220-cm^{-1} mode over the 370-cm^{-1} mode when 413-nm excitation is compared to 458-nm excitation. This type of behavior mimics the observations of Ondrais et al.[10] and Irwin et al.[11] (It turns out, however, that this type of relative enhancement pattern does *not* necessarily imply that a blue-shifted charge-transfer transition is present; see Figure 9 for example.)

The REP of this mode is given in order to simulate the observations of Irwin et al.[11] Their results show a *relative* enhancement of the 220-cm^{-1} mode over other low-frequency modes as the laser excitation is changed from 457.9 to 413.1 nm. As we shall see, this relative enhancement does *not* necessarily imply the separate charge-transfer band assumed in Figure 2 for illustrative purposes.

The associated absorption band shapes ($A_\pi(\bar{\nu})$ and $A_{CT}(\nu)$) are obtained by the inverse transform and summed according to eq 7. It is found by least-squares analysis that $Z = 0.095$ yields the observed absorption band shape, $A(\bar{\nu})$, and the relative extinction coefficients follow according to eq 8. These results are plotted on an absolute scale of extinction coefficients in Figure 2, right. Finally, scaling the individual REP's using their respective absorption bands and the forward transform leads to values of $S_{1357} = 0.05$, $S_{370} = 0.012$, and $S_{220} = 2.14$ for the coupling strengths of interest. The relatively large value for S_{220} may well be reasonable for a localized electronic excitation associated with a charge-transfer transition (i.e., a delocalized $\pi-\pi^*$ excitation couples weakly to many nuclei while a charge-transfer excitation couples strongly to only a few nuclei).

It is also worthwhile to note at this point that in order to maintain a constant Raman intensity, the coupling strength must increase *quadratically* as the extinction coefficient is decreased linearly (this can be seen directly from eq 1–4). Thus, a factor of ten decrease in ϵ ($\epsilon_{CT} \sim 0.1\epsilon_\pi$) implies an increase of 100 in the coupling strength. In addition, S also shows strong dispersion with respect to the Raman frequency[22,24] and must increase rapidly at low frequency in order to maintain a fixed Raman intensity. These two effects are acting in concert in the present example to effectively increase the coupling strength of the iron–ligand mode even though its absolute Raman cross section falls below that of the 1357-cm^{-1} mode. A more detailed discussion of these points will be made in our analysis of the actual myoglobin data.

C. Ensemble Effects. The problem of the ensemble average is a notorious one that is quite often ignored in the analysis of condensed-phase Raman data. The difficulty arises due to the fact that, almost without exception, the theory is initiated via complex scattering amplitudes at the single molecule level and the weighted ensemble averages must be carried out at the amplitude squared intensity level. The transform theory is no exception to this general difficulty. Nevertheless, calculations can be made using computer simulations in order to estimate the magnitude of ensemble effects.

We have previously[22] discussed some aspects of this problem with respect to the transform theory and presented some quantitative calculations for a site-broadened absorption band and fixed Raman frequency. Here we wish to stress the dispersion in these effects as the Raman frequency is varied. This is a particularly important problem for the heme proteins, since they span such a wide range of Raman frequencies and since comparisons of absolute intensity between low- and high-frequency modes may lead to useful and important information about the active-site structure.

We have recently[24] explored in great detail the temperature effects on the REP's of both Stokes and anti-Stokes scattering of the low-frequency modes of cytochrome *c*. The detailed expressions needed for the analysis of the anti-Stokes scattering and the explicit form of the ensemble average are not given in the present work for reasons of simplicity. We remark only that the correct formal expression for the transform theory at finite temperature must involve the separate electronic subspectra (or their sums) composed of transitions from well-specified initial states to all final states in the resonant electronic absorption band. As a result, approximations must be made in order to implement the transform technique in a practical sense. The effects of the approximations leading to eq 1–4 for finite temperature analysis have been discussed in great detail by Chan and Page.[28b] We will not consider them further here, except to note that the preservation of centroid and integrated area of the separate subspectra (i.e., the first and zeroth moments of all thermal subspectra remain fixed) tends to minimize the error due to the approximations involved in thermal averaging.

On the other hand, inhomogeneous site broadening can cause a significant (Raman frequency dependent) underestimate of the single-molecule scattering intensity (which translates into an overestimate of the coupling strength) if eq 1–4 are used without regard for ensemble broadening effects. The magnitude of the effect is due primarily to the fact that differing sites (or conformations) can have different sets of transition energies that do *not* all share the same centroid (first moment). As the Raman frequency becomes smaller such effects are more pronounced as we now demonstrate.

We proceed by using a computer to model an absorption band having varying degrees of site broadening convoluted into the spectrum so as to yield a fixed band shape (the shape is set to model the Soret band of deoxymyoglobin as closely as possible). We then perform the transform operation, as specified in eq 1–4, on both the ensemble-averaged spectrum and the separate and appropriately weighted subspectra. The incorrect results, obtained by ignoring the ensemble effects, closely resemble the more formally rigorous results when only line shapes are considered. (The subtle differences in line shape that do appear may ultimately result in a useful experimental method for estimating the magnitude of site broadening.) However, when the absolute scattering intensities are also considered, it becomes clear that ignoring the ensemble effects leads to an underestimate of the single-molecule scattering intensity.

The results of our calculations are summarized in Figure 3. Here we plot the ratio of S^* (correctly determined) to S (incorrectly determined) as a function of Raman mode frequency for some typical Gaussian site distributions (σ is a half-width at $1/\sqrt{e}$). It is important to note that for mode frequencies much greater than the distribution width, very little error is incurred by ignoring the ensemble effects. On the other hand, for low-frequency modes (on the order of σ_{site}) we must be prepared to acknowledge ensemble effects as a potentially serious source of error which, nevertheless, can be estimated by use of Figure 3. We will proceed with our analysis of the Mb and Hb data in section IV as if the site broadening were negligible (i.e., we determine S not S^*). In the Discussion section we will estimate σ_{site} and use this to revise our values of the coupling strength.

III. Experimental Section

The Mb samples are obtained from Sigma Chemical Co. (sperm whale type II) and purified by using column chromatography (Sephadex G-25, equilibrated with 0.05 M sodium phosphate buffer, pH 7). Ammonium

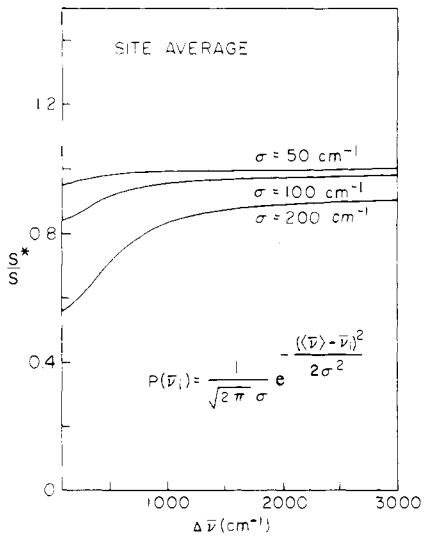

Figure 3. A plot of the true value of the coupling strength (S^*) over the apparent value (S) when inhomogeneous broadening is operative. The apparent value, S, is obtained by transforming the observed absorption line shape without intensity. The correct value, S^*, is obtained by first deconvoluting the (known) distribution from the absorption band shape, transforming and squaring as in eq 1–4, and then reconvoluting the same distribution back into the Raman intensity before scaling to the observed intensity. A Gaussian site distribution has been utilized with various values of the broadening parameter σ. The quantity $\langle\bar{\nu}\rangle$ represents the centroid of the observed absorption band shape. $P(\bar{\nu}_i)$ represents the probability of finding the heme in "site" i having an absorption spectrum with centroid at $\bar{\nu}_i$. Notice that there is dispersion in this effect with the Raman mode frequency, $\Delta\bar{\nu}$. When $\Delta\bar{\nu} \lesssim 2\sigma$, fairly large overestimates of the coupling strength can arise if no attention is given to the effects of the site distribution.

sulfate (1.0 M) is added as an internal standard in order to quantify the resonance Raman cross section. (The total cross section of the 980-cm^{-1} band of the standard is $\sigma_{980} = 3.4 \times 10^{-29}$ cm^2/sr·molecule at 413.1-nm excitation, which has been measured elsewhere[23]). The Hb samples are obtained from whole blood by the technique of Gibson et al.[39] The samples are deoxygenated in a tonometer, and small quantities of sodium dithionite are added under nitrogen atmosphere in order to reduce the samples to the deoxy form. The met Mb samples are formed by oxidizing with potassium ferricyanide and the excess ferricyanide is separated out by passing through the Sephadex G-25 column. The concentration of the samples is 30–40 or 300 μM, depending on whether the excitation frequency is in or out of resonance. After addition of sulfate, the pH of the samples is found to be 6.5. A 90° Raman scattering geometry is employed and the samples are characterized before and after the scattering experiments by their optical absorptions (Perkin-Elmer Model 320). During the experiment, the samples are kept at 288 K by use of a thermoelectric cooler or at 110 K by use of a special cryostat with the sample in contact with a liquid nitrogen reservoir.

The Raman spectra are accumulated with use of a Spex 1403 double monochromator, RCA 31034 phototube, and PAR 1109 photon counter all interfaced to a DEC Minc 11/23 computer system. This same computer is also interfaced to the PE 320 spectrophotometer in order to allow digital acquisition of the absorption spectra for transform analysis. The laser-excitation frequencies range from 408 to 458 nm and are generated by using a Spectra-physics 171 argon ion laser to pump a coherent CR-599 dye laser with stilbene 1 and stilbene 3 dyes. The cross section of the 980-cm^{-1} standard band at the various laser frequencies is found by scaling the 413.1-nm cross section by $(\bar{\nu} - \bar{\nu}_a)^3\bar{\nu}$ as is appropriate for photon counting detection of a nonresonant internal standard. Typical running conditions for the Raman spectra are as follows: 4-cm^{-1} slit width, 2-cm^{-1} step size, 15-mW power at the sample, 5-s counting time per channel.

Typically we isolate a given electronic transition (e.g., Soret band) in order to perform the transform operations (the effect of additional, nonresonant transitions is small and can be modeled by a constant background, if necessary). In Figure 4 we display the Soret band of deoxy Mb (curve 1) and two types of extensions on the high-energy side (Lorentzian, curve 2; Gaussian, curve 3). The respective REP's for the

(39) Gibson, O. H. *J. Biol. Chem.* **1970**, *245*, 3285.

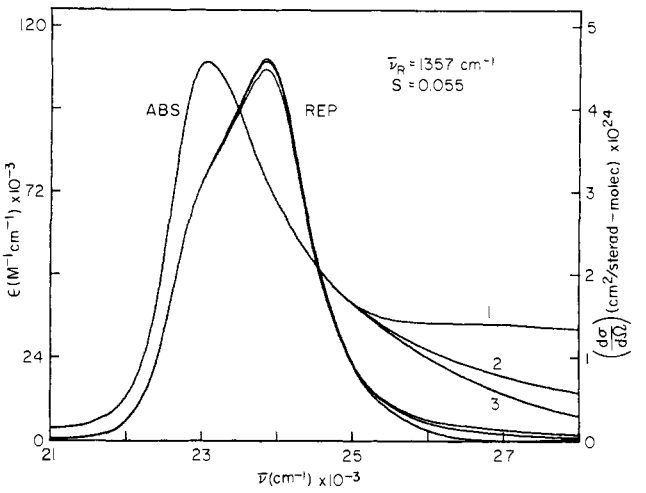

Figure 4. The effect of changing the blue tail of the absorption band shape is shown to have little effect on the REP calculation. Notice that all calculations are done at the absolute cross-section level. Curve 1 is the observed band shape of deoxy Mb. Curves 2 and 3 are respectively Lorentzian and Gaussian extensions, continuously attached. The REP associated with curve 1 has the smallest intensity at the maximum.

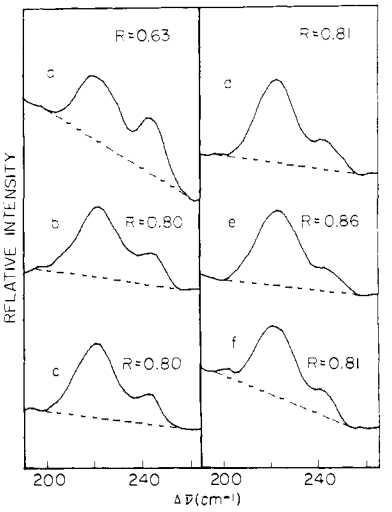

Figure 5. The Raman line shape of the 220–240-cm^{-1} mode at various laser excitation frequencies. The ratio R, given in each portion of the figure, is the fraction of the total area that is associated with the 220-cm^{-1} mode. These ratios were obtained by least-squares analysis of the line shape. The laser frequencies are (a) 21 842 cm^{-1}, (b) 22 650 cm^{-1}), (c) 23 041 cm^{-1}, (d) 23 585 cm^{-1}, (e) 24 016 cm^{-1}, and (f) 24 240 cm^{-1}.

1357-cm^{-1} mode (obtained by use of eq 1–4) are also shown. It is clearly seen that the details of the approach to zero on the blue side of the absorption band do not significantly affect the calculations. In this work we use the Lorentzian tail (continuously attached) to extend our band shapes to the base line on the blue side of the transition.

For analysis of the Raman exctation profiles we use the computer to calculate the area of the Raman peaks and correct for the differential reabsorption of scattered light between the sample and the standard band. This small correction is accurately estimated by using the Stokes and anti-Stokes scattering of the standard.[24] Since the nonresonant standard band should have its anti-Stokes/Stokes intensity ratio given by the Boltzmann factor, any deviation in this ratio is ascribed to differing amounts of reabsorption. Use of the Stokes and anti-Stokes scattered light frequencies and the respective extinction coefficients leads to an accurate measure of the effective scattering path length (typically 0.3–0.5 mm). This, in turn, allows calculation of the reabsorption correction for the resonant scattering with respect to the standard band.

In the case of the 220-cm^{-1} mode of Mb and 216-cm^{-1} mode of Hb it is difficult to determine the true base line and Raman line shape in order to calculate the integrated intensities. In Figure 5 we display some typical line shapes for the 220-cm^{-1} mode of Mb excited at various laser frequencies. There is clearly a shoulder in the spectra at ca. 240 cm^{-1}. In our analysis, we calculate the entire area under the feature at 220–240 cm^{-1} as shown by the dotted line. The total cross section for scattering

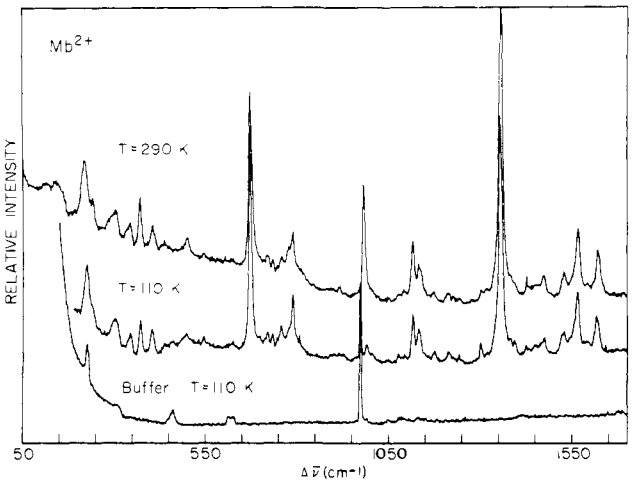

Figure 6. The full Raman spectrum of deoxy Mb with use of a laser excitation of 434 nm, in resonance with the Soret absorption band. The spectra are unsmoothed, raw data. The lower two spectra were accumulated at cryogenic temperatures with use of a liquid nitrogen cold finger. Our original plan to cross-check the 220-cm^{-1} REP at low temperature had to be modified due to the lattice mode of ice that appears in the same region of the spectrum. The main features of interest in the present study are found at ca. 150, 220, 370, 674, and 1357 cm^{-1}.

light into this frequency range is the plotted quantity in the next section. We note at this point, however, that the shoulder at 240 cm^{-1} is not necessarily associated with the Fe–N_{His} vibration. Least-squares fitting of Lorentzians to the line shapes in Figure 5 results in the fraction of total area that we can assign separately to the 220-cm^{-1} mode (ca. 80%). On the wing of the resonance, at 458 nm, we find a slight disparity in this fraction which may be due to weak non-Condon effects or simply to the reduced signal-to-noise levels. Overall, we estimate the errors to be in the ±15% range.

IV. Results

In Figure 6 we display the full resonance Raman spectrum of deoxymyoglobin obtained by using 434-nm laser excitation. The modes of interest in this particular study involve the histidine–iron–porphyrin system and are located at 150, 220 (Fe–N_{His}), 370, 674, and 1357 cm^{-1} (ring breathing).

Raman spectra at cryogenic temperatures are also accumulated in an attempt to cross-check the excitation profile of the 220-cm^{-1} mode at low temperature. However, as can be seen in the lower curve, severe difficulties arise in the low-temperature experiment due to interference from the Raman scattering of ice. This same ice mode (at ca. 227 cm^{-1}) probably accounts for some of the earlier reports of line narrowing and shifting of the Fe–N_{His} mode at cryogenic temperature.[7,8]

In Figure 7 we present the REP's of the ring-breathing modes of deoxy Mb. Notice that all data are placed on an absolute cross-section scale by comparison to the sulfate internal standard. The solid lines through the data points represent a transform fit to the data with use of the Soret band of Figure 4 and eq 1–4 as discussed in the previous sections. In the case of the 674-cm^{-1} mode only a single free parameter (i.e., $S = 0.035$) has been utilized to achieve an essentially perfect fit to the data. This value of S is typical of those we have found for coupling to the Soret resonance (see Table I).

The Raman data for the 1357-cm^{-1} mode, on the other hand, have presented us with some difficulty. The fit given in Figure 7 is reasonable but below our expectations based on previous experience. In fact, we have optimized the fit by utilizing some weak non-Condon[22,23] scattering amplitude ($Ca \cong -0.083$, see ref 23). Nevertheless, discrepancies still remain that we tentatively assign to inhomogeneous ensemble effects. As we have seen previously,[23] incorrect ensemble averaging can lead to subtle errors in the shape of the REP similar to those we experience in Figure 7. Further work on this problem is now underway; one promising aspect is that the transform method may ultimately allow the deconvolution of inhomogeneous contributions to the absorption line shape when the REP is carefully measured.

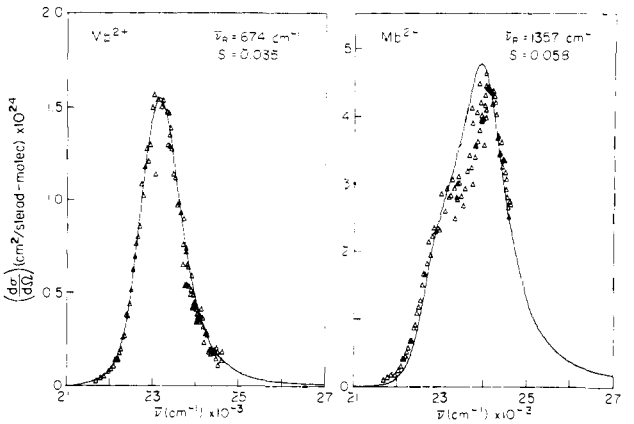

Figure 7. The REP's of the 674- and 1357-cm^{-1} ring modes of deoxy Mb. All data are plotted on an absolute Raman cross-section scale by reference to the internal sulfate standard at 980 cm^{-1}. The solid curve in the REP of the 674-cm^{-1} mode is the result of a one-parameter fit ($S = 0.035$) using eq 1–4. In the case of the 1357-cm^{-1} mode we have tried to optimize the fit by the addition of some weak non-Condon coupling. This coupling can be described by an additional parameter (see ref 23). Our optimum fit shown in the figure finds $S = 0.058$ and $C_a = -0.083$ which corresponds to a <1% non-Condon effect at the intensity level. Given the success of our previous attempts at fitting REP's by using the transform, we feel that the fit of the 1357-cm^{-1} REP can still be improved. The deconvolution of inhomogeneous broadening from the absorption spectrum appears to be a promising avenue that is currently being explored. (Note that the low-frequency modes do not have enough resolution in their REP's to be sensitive to the subtle variations in the shape of the REP that signal the inhomogeneous effects.)

Table I. Coupling Strengths for Various Heme Proteins

protein	mode, cm^{-1}	ρ^a	S	$C_a{}^b$	ref
deoxy Mb	150	0.40	0.04–0.09[c]	0.0	this work
	220	0.15	0.06–0.16[c]	−0.075	this work
	370	0.125*	0.020	0.0	this work
	674	0.16	0.035	0.0	this work
	1357	0.17	0.058	−0.083	this work
deoxy Hb	216	0.125*	0.03–0.06[c]	0.0	this work
aquomet MB	248	0.125*	0.09–0.15[c]	0.0	this work
	674	0.125*	0.043	0.0	this work
	1370	0.125*	0.051	0.0	this work
ferricyto-chrome *c*	125–325	0.14	0.017[d]	0.0	24
	325–545	0.14	0.017[d]	0.0	24
	1372	0.14	0.023	0.0 ± 0.05	23
ferrocyto-chrome *c*	135–325	0.14	0.03[d]	0.0	24
	325–545	0.14	0.021[d]	0.0	24
	1362	0.14	0.033	−0.13	23
cytochrome P-450					
m^{0s}	351	0.125*	3.0[e]	0.0	57
m^0	676	0.14	0.04	0.0 ± 0.05	57
	1372	0.15	0.051	0.0 ± 0.05	57

[a] The depolarization ratios used in the transform fit of experimental data (the asterisk denotes the estimated value of ρ). [b] C_a is the ratio of non-Condon to Condon amplitude (see ref 22 and 23). [c] Exact value depends on the size of inhomogeneous site broadening. [d] Einstein approximation includes about ten modes in each range, therefore S (for each mode) is equal to $\bar{S}/10$ (see ref 24). [e] This result is obtained by assuming a charge-transfer transition underlies the Soret region of P450. The assumed oscillator strength is ca. 0.1 that of the Soret band.

In Figure 8 we present the REP of the 220-cm^{-1} (Fe–N_{His} mode of deoxy Mb ($\rho \simeq 0.2 \pm 0.1$). The analogous mode in R and T states of deoxy Hb has been the object of numerous recent Raman investigations. In the left-hand panel we display the data on an absolute scale along with the transform fit using the Soret absorption band. The dotted line represents the pure Condon (A term) transform while the solid line has invoked a very small

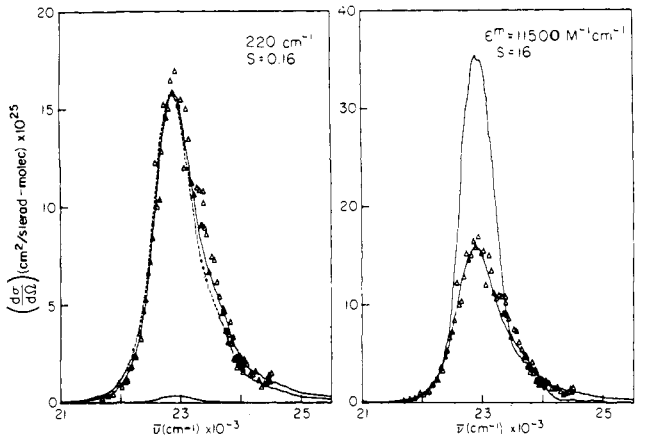

Figure 8. The REP of the 220-cm^{-1} mode of deoxy Mb that has been assigned to the Fe–N_{His} stretching frequency. The fits on the left-hand side correspond to pure Condon scattering (dashed line) and the addition of slight (<1%) non-Condon coupling (solid line through data). The value for $S = 0.16$ is probably an overestimate due to inhomogeneous ensemble effects as discussed in the text. The thin solid line at the bottom of the figure is the predicted overtone scattering intensity for $S = 0.16$. On the right-hand side of the figure, we have assumed a buried charge-transfer band ($\epsilon_{CT} \simeq 0.1\epsilon_x$) that mimics the position and line shape of the Soret transition. Under this circumstance $S = 16$ in order to fit the data points. Due to the large value of S, strong overtone scattering is predicted which is unobserved. As a result, we reject the assumption of an underlying charge-transfer resonance that is enhancing the Raman scattering of the Fe–N_{His} mode.

amount of non-Condon (B, C term) interference ($C_a = -0.075$, <1% at intensity level) in order to give slightly improved fits.

The important things to notice about the left-hand side of Figure 8 are the following: (1) The Fe–N_{His} mode appears to be in resonance with the Soret band and *not* with a separate underlying charge-transfer band. (2) The coupling strength, $S = 0.16$, found by scaling the absolute intensity appears to be significantly *larger* than the porphyrin ring modes! (3) The overtone scattering intensity predicted by the transform theory with $S = 0.16$ is given by the thin solid line at the bottom of the figure and is probably too weak to be detected (this agrees with the observed absence of scattering in the 440-cm^{-1} region of the spectrum).

On the right-hand side of Figure 8 we have explored the possibility that there may be an underlying charge-transfer band which (coincidentally) mimics the Soret band shape and position, yet has a reduced oscillator strength. We have chosen the maximum of the extinction coefficient for this hypothetical charge-transfer band to be 10% that of the Soret (i.e., $\epsilon^m = 11500$ M^{-1} cm^{-1}) which might be considered reasonable for such a transition.

Since the fundamental scattering scales as $S\epsilon^2$, we see that a decrease of ϵ by a factor of 10 will increase S by a factor of 100! This important and general result leads to a value of $S = 16$ for the Fe–N_{His} mode if it is indeed coupled to a charge-transfer transition having the assumed oscillator strength. (Smaller values of ϵ obviously lead to even larger values of S.) As one might imagine, such a large value of the coupling strength must imply strong overtone scattering. In fact, the overtone scattering[28] scales as $S^2\epsilon^2$, so it is even larger than might otherwise be expected once S rises above unity. The thin solid line above the 220-cm^{-1} data points on the right of Figure 8 is the predicted overtone scattering intensity if the Fe–N_{His} mode were coupled to a charge-transfer band having an extinction maximum of 11 500 M^{-1} cm^{-1}. Since such intense overtone scattering is not observed, it appears that the Fe–N_{His} mode is coupled directly to the Soret transition with a coupling strength on the order of 0.16.

Since this result is apparently at variance with the observations of others,[10,11] we have displayed in Figure 9 the high-resolution REP of the 220-cm^{-1} mode along with another low-frequency mode at 370 cm^{-1}. The solid lines through the data points are again obtained by using the transform theory ($S_{370} = 0.02$). The slight amount of non-Condon contribution to the 220 cm^{-1}

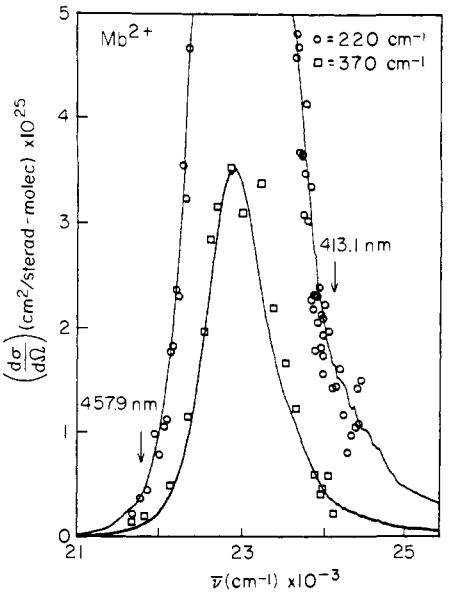

Figure 9. We display in high resolution the REP's of the 220-cm^{-1} mode and the 370-cm^{-1} mode. Both solid curves are the result of the transform fit with use of S as a scaling parameter ($S_{370} = 0.02$). The arrows represent the laser excitations used by Irwin et al.[11] This demonstrates that the relative intensity of the 220-cm^{-1} mode is larger than that of other low-frequency modes (e.g., 370 cm^{-1}) when spectra taken at 413.1 nm are compared with those taken at 457.9 nm. Nevertheless, both modes are coupled to the Soret resonance.

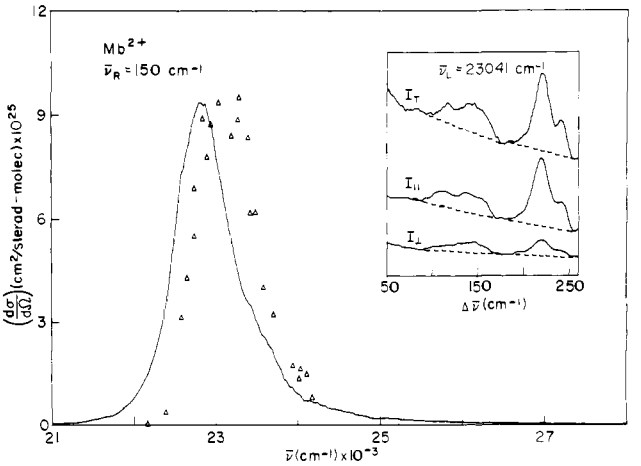

Figure 10. The REP of the 150-cm^{-1} feature of deoxy Mb. The solid curve is the result of a transform of the Soret band scaled by using $S = 0.09$. Notice that the data points are distinctly shifted with respect to the predicted REP. The insert shows the total scattering in the 50–250-cm^{-1} region (top) as well as the parallel and perpendicular components of the scattering accumulated in separate runs.

scattering amplitude may account for some additional asymmetry in its REP line shape (see Figure 8). Nevertheless, even without this effect, the overall asymmetry of the respective REP's, along with stronger coupling for the 220-cm^{-1} mode, leads directly to the previously noted[10,11] difference in relative scattering intensities using 413.1- and 457.9-nm excitation. The fact that the 220-cm^{-1} mode is relatively more intense than the 370-cm^{-1} mode when 413.1-nm excitation is used does *not* imply that the 220-cm^{-1} mode is coupled to a charge-transfer resonance to the blue of the Soret band.

In Figure 10 we display the results of a preliminary investigation of the interesting feature at ca. 150 cm^{-1} in the Mb spectrum. This feature has been reported to undergo changes in frequency in Hb systems that parallel those of the 220-cm^{-1} mode.[40] The

(40) Ondrais, M. R.; Rousseau, D. L.; Shelnutt, J. A.; Simon, S. R. *Biochemistry* **1982**, *21*, 3428–3437.

insert of Figure 10 shows, in high resolution, that this feature may in fact be a doublet with depolarization ratio $\rho \simeq 0.4 \pm 0.1$. It is also seen that the profile is significantly shifted to the blue of the pure Condon (A term) transform of the Soret band. An attempt to fit this REP has also been made by using significant non-Condon (B, C term) interference effects. Our best fit under these circumstances is still not satisfactory.

An obvious alternative explanation for the REP of the feature at 150 cm^{-1} involves construction of a shifted charge-transfer band underlying the Soret transition. As discussed previously, such a transition ($\epsilon^m = 11\,500\ M^{-1}\ cm^{-1}$) must be rather strongly coupled in order to generate observable low-frequency Raman scattering. Overtone scattering will also be predicted under such circumstances and, in the case at hand, a candidate for the overtone happens to be present at ca. 300 cm^{-1}. We have also monitored the REP of the 300-cm^{-1} mode and have attempted to fit both the 150- and 300-cm^{-1} REP's simultaneously (in the Condon limit) using a single value of S. Since the fundamental and overtone scale as $S\epsilon^2$ and $S^2\epsilon^2$, respectively, a unique value of S must emerge if this type of analysis is correct. Using such a simultaneous fitting procedure we find that $S = 5.8$ yields an acceptable (although not perfect) fit to both the 150- and 300-cm^{-1} modes. Such a large value of S would not be unreasonable for a highly localized charge-transfer excitation which is coupled to only a few nuclei. More experimental work is clearly needed in order to explore the charge-transfer possibility more fully. Additional explanations for the behavior of the 150-cm^{-1} mode may also emerge. (It is unfortunate that the isotopic labeling studies did not include the 150-cm^{-1} region.)

A variety of other experiments involving deoxy Hb and met Mb have also been carried out (see Table I); these will be reported in detail elsewhere. The REP of the Hb 216-cm^{-1} mode is essentially identical in shape with that of the 220-cm^{-1} mode of Mb. However, the magnitude of the scattering is decreased by approximately a factor of 2. This signals a weaker coupling of $Fe-N_{His}$ to the $\pi-\pi^*$ transition in T-state Hb when compared to deoxy Mb. A possible explanation for this behavior will be presented in the next section.

V. Discussion

A. General Analysis. Before proceeding further we wish to clarify why such a large value for S can be expected for a low-frequency mode without a concomitant increase in its Raman intensity (e.g., the value of $S_{220} = 0.16$ is much larger than $S_{1357} = 0.058$ and yet these modes have similar intensities). This occurs due to a previously described[22,24] dispersion phenomenon that arises from the opposite phasing found in the Condon scattering amplitude (see eq 3). As the Raman frequency, $\bar{\nu}_a$, decreases it can be seen directly from eq 3 that $\alpha_T(\bar{\nu})$ will approach zero. Thus, larger and larger values of S_a are needed in eq 1 in order to maintain observable Raman intensity.

This effect can be quite dramatic[24] and strongly discriminates against the observation of low-frequency modes unless rather large coupling is present. Figure 11 displays the coupling strength vs. Raman frequency dispersion curves obtained by using laser excitation near the Soret maxima of cytochrome c and myoglobin. These curves represent the magnitude of the coupling strength needed in order to observe Raman scattering of fixed intensity (see ref 22 and 24 for more details). Here, we only wish to demonstrate the general phenomenon and rationalize why such a large value of S is needed to explain the observed Raman intensity of the 220-cm^{-1} mode. We will take up separately the question of why the $Fe-N_{His}$ mode is coupled to the $\pi-\pi^*$ Soret transition and what structural parameters might lead to its observed magnitude (see below).

We have seen in this and in previous work[23,24] that the transform theory works extraordinarily well in predicting the REP line shapes and Raman intensities of heme proteins. The REP of the 1357-cm^{-1} mode in Figure 7 appears to be a notable exception to the quality of fits we have come to expect. One reason for our inability to perfectly match the REP line shape in Mb is possibly due to the inhomogeneous nature of the Mb molecule (by this we mean the conformational substates[36,41,42] that have come to be associated with Hb and Mb).

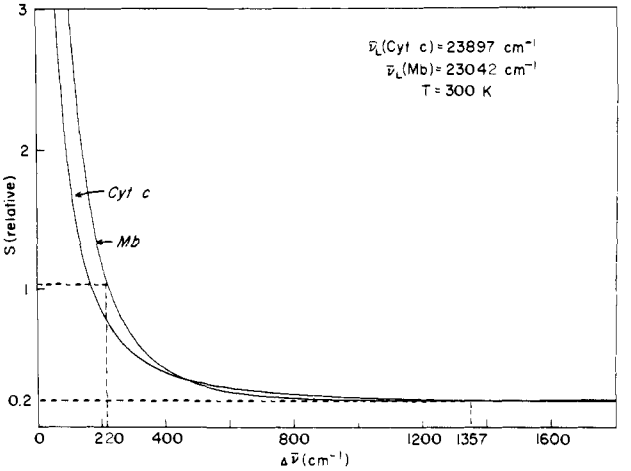

Figure 11. The dispersion of the coupling strength is given for deoxy Mb and ferrocytochrome c when the laser excitation is near the peak of the Soret band. These curves should be interpreted as the coupling strength needed to maintain a given (unit) Raman intensity as the Raman mode frequency is varied. The product of these curves with the Raman spectrum at the given laser excitation yields the "coupling strength spectrum" (see ref 24 for details). Notice that the dispersion for deoxy Mb is rather steep at low frequency; this is why large coupling strengths are necessary in order to match the observed Raman intensity of the 220-cm^{-1} mode.

Since the effect of an inhomogeneous distribution of substrates is directly folded into the absorption spectrum, we must be prepared to deconvolute this distribution prior to application of eq 1–4. This same distribution must then be reapplied to the Raman intensity calculation in order to generate the true REP (i.e., use of the inhomogeneously broadened absorption band in eq 1–4 is incorrect in the sense that the average over initial states of the system is being applied at the Raman amplitude level rather than at the Raman intensity level). The identical problem arises in the thermal average but is much less severe since the first moments of all the thermal subspectra remain fixed[24] in marked contrast to an inhomogeneous site distribution.

Preliminary results indicate[23] that the REP line shape predicted for the 1357-cm^{-1} mode will more closely match the data once an inhomogeneous site distribution is deconvoluted from the Soret band. Detailed work on this effect is currently under way in our laboratory in order to quantify the magnitude of the (assumed Gaussian) site distribution function in the Mb and Hb systems. The prospects appear quite promising that if both the REP and absorption band shapes are carefully monitored, the inhomogeneous distributions can be obtained directly from a simultaneous analysis of the data. Our previous work[23,31] indicates that the heme chromophore of cytochrome c is not significantly influenced by inhomogeneous effects. This may be a direct reflection of the covalent bonding at the heme periphery in cytochrome c which "locks" the chromophore into a more homogeneous protein environment compared to that of Hb and Mb.

As pointed out earlier, inhomogeneous broadening can have important effects on the Raman intensity as well as the REP line shapes if the distribution widths are on the order of the Raman frequency. Thus, the scattering intensities of low-frequency modes tend to be more strongly affected than those of high-frequency modes. If we use Figure 3 as a guide, we expect that our value for $S_{220} = 0.16$, obtained directly from the transform, is an overestimate that will be reduced in the event that significant inhomogeneous effects are found to be present in the Mb system. Consideration of this, as well as the line-shape analysis of Figure 5, suggests that S_{220} lies with high probability in the range 0.06–0.16. Nevertheless, the magnitude of this coupling is sur-

(41) McCammon, J. A.; Karplus, M. *Acc. Chem. Res.* **1983**, *16*, 187.
(42) Austin, R. H.; Beeson, K. W.; Eisenstein, L.; Frauenfelder, H.; Gunsalus, I. C. *Biochemistry* **1975**, *14*, 5355.

prisingly large given that the iron–histidine bond is not obviously involved in the porphyrin π-electron network which is responsible for the Soret transition (recall that the porphyrin ring modes themselves have typical S values of ca. 0.04, see Table I). We will discuss below a possible mechanism that directly couples the π–π^* porphyrin excitation to the Fe–N_{His} mode.

The polarization properties of the 220- and 150-cm^{-1} modes also deserve comment. Our measurements so far indicate $\rho_{220} \simeq 0.2 \pm 0.1$ and $\rho_{150} \simeq 0.4 \pm 0.1$ with the possibility that some weak dispersion is present throughout the Soret resonance. The depolarization ratio measurements are particularly difficult for the low-frequency Mb and Hb modes due to the broadness of the 150-cm^{-1} feature and interference from the 240-cm^{-1} mode. Thus, small errors in base line determination or deconvolution of the perpendicularly polarized component can lead to large errors in ρ. Nevertheless, it appears that these modes are not typical polarized A_{1g} modes which are expected to have depolarization ratios of 0.125 in D_{4h} symmetry. On the other hand, if the electron–nuclear coupling of these modes proceeds preferentially via the x- *or* the y-polarized Soret transition moments such large values of ρ might be expected (i.e., $\alpha_{xx} \gg \alpha_{yy}$ and $\alpha_{zz} \simeq 0$ will lead to $\rho \simeq 0.33$). A structural picture that explicitly accounts for such effects is discussed below. Further, more precise measurements of the depolarization ratio and its frequency dependence are presently under way.

The REP of the 150-cm^{-1} feature remains to be explained. As discussed above, it is conceivable that this mode could be coupled to an underlying blue-shifted charge-transfer transition. It is clearly of interest to assign this feature to some specific vibrational motion of the heme ligand system. The report[40] that the 150-cm^{-1} mode shows behavior that parallels the 220-cm^{-1} mode in various Hb systems suggests that additional labeling experiments may be necessary.

B. A Coupling Hypothesis. There is a rather extensive literature that has developed on the subject of Hb cooperativity and the specific (heme localized) structural effects that are involved. We do not wish to review the details of the various approaches here, but we simply remark that one feature common to many current models involves stabilization of the R-state oxy complex with respect to the T-state oxy complex[43,44] (see Figure 12A). This type of stabilization and its relationship to the resonance Raman data[40,45] are usually explained by invoking the "tilt" of the proximal histidine (His F8) and the non-bonding repulsive interaction that arises between the histidine carbons (C_δ–H and C_ϵ–H) and the porphyrin nitrogens (N_3 and N_1). This tilt is thought to account for the lowered deoxy T-state Fe–H_{His} Raman mode frequency[4,45] as well as stabilization of oxy R state with respect to oxy T state (thus partially accounting for the higher R-state affinity[40,44,45]).

Other models have invoked the deprotonation or hydrogen bonding of the proximal histidine (N_δ–H) as a possible means by which gross conformational structure can strongly influence the reactivity of the heme system.[5,46-48] Unfortunately, this type of model has not received a great deal of attention in much of the current Raman work. However, Ondrais et al.[40] have observed solvent effects on the Raman spectra of model compounds that they feel argues against participation of proximal histidine deprotonation in the energetics of cooperativity.

We delineate below some of the key Raman observations that must be simultaneously explained by any successful model of the (heme localized) structure function relationship in Hb and Mb: (1) strong coupling of the Fe–N_{His} mode to the Soret resonance of deoxy Mb and deoxy Hb (this work); (2) higher Fe–N_{His} mode frequency in the deoxy R state than in the deoxy T state (ref 3, 4, and 45); (3) inverse relationship between changes in the Fe–N_{His} mode frequency and porphyrin ring breathing mode, ν_4 (ref 40 and 49); (4) weaker Fe–N_{His} Raman scattering (*ca.* factor of two) from the deoxy T state than from the deoxy R-state Hb or deoxy

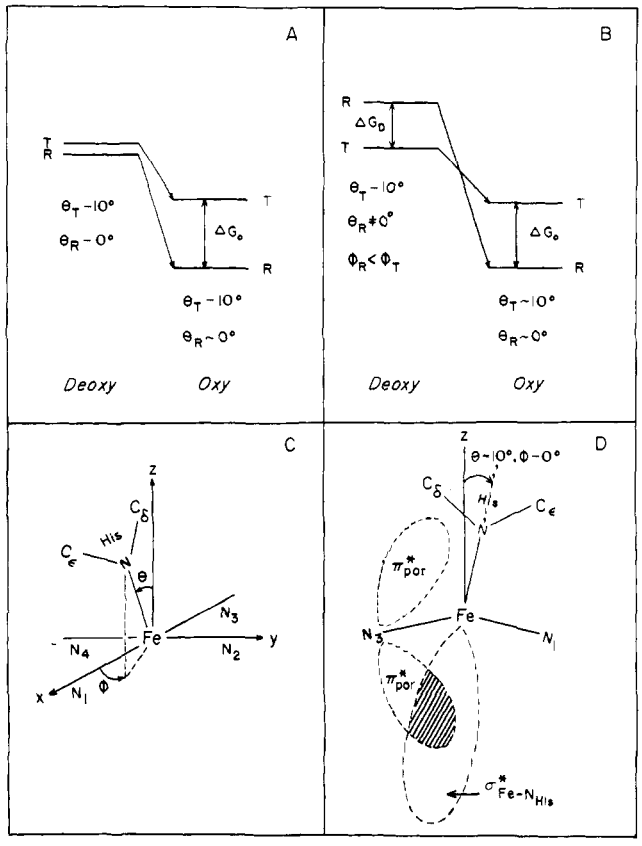

Figure 12. A diagrammatic representation of the coupling hypothesis presented in the text. (A) The free energy diagram for the R and T forms of Hb which attributes most of the difference in local free energy to strain energetics in the oxygenated forms of the protein. (B) The free energy diagram appropriate to the hypothesis presented in the text. Note that the $\theta_R \neq 0$, $\phi_R < \phi_T$ conditions imply a heme localized increase in electron–electron repulsion energy for the deoxy R state (see D). (C) The polar and azimuthal angles θ, ϕ are defined by the Fe–N_{His} vector with respect to the heme nitrogens and the heme normal. (D) The extreme case $\phi \sim 0°$ is presented in order to demonstrate how $\sigma^*_{Fe-N_{His}}$–π^*_{por} mixing may occur. The electron–electron repulsion interaction between the single electron in $\sigma^*_{Fe-N_{His}}$ and the filled π_{por} electron density (not shown) on the heme nitrogens can lead to $\sigma^*_{Fe-N_{His}} \rightarrow \pi^*_{por}$ electron donation. The π_{por}–π^*_{por} excitation, on the other hand, can lead to direct harmonic coupling of the Fe–N_{His} mode via the orbital mixing of π^*_{por} and $\sigma^*_{Fe-N_{His}}$. It should be emphasized that the free energy diagrams represent the *local* heme energetics that may be responsible for the different oxygen affinities of the R and T structures. These diagrams are *not* meant to represent the global free energy changes associated with the quaternary structure alterations. The global changes are driven by both enthalpic and entropic forces which can presumably result in regions of increased local energy (e.g., the deoxy heme in R-state Hb). Notice that the global T → R transition will contain four heme localized (enthalpic) terms. Those hemes with bound oxygen will each decrease their energy by ΔG_0 while the deoxy heme(s) will increase its energy by ΔG_D (see **B**). Thus, the heme-localized contribution to the global free energy change would go as $(4 - n)|\Delta G_D| - n|\Delta G_0|$ if the T → R transition takes place after n oxygen molecules are bound. Obviously, this contribution becomes more and more favorable to the T → R transition as n increases (ΔG more negative) and could help explain the thermodynamics of cooperativity. The so-called free energy of cooperativity is found from the difference in the local O_2 binding affinity between the R- and T-state hemes and is given by $|\Delta G_D| + |\Delta G_0| \simeq 3.4$ kcal.

(43) Gelin, B. R.; Karplus, M. *Proc. Natl. Acad. Sci. U.S.A.* **1977**, *74*, 801–805.
(44) Perutz, M. F. *Proc. R. Soc. London, Ser. B* **1980**, *208*, 135–162.
(45) (a) Friedman, J. M.; Scott, T. W.; Stepnoski, R. A.; Saito, M. I.; Yonetani, T. *J. Biol. Chem.* **1983**, *258*, 10564. (b) Friedman, J. M.; Rousseau, D. L.; Ondrais, M. R.; Stepnoski, R. A. *Science* **1982**, *218*, 1244–1246.
(46) Chevion, M.; Salhany, J. M.; Castillo, C. L.; Peisach, J.; Blumberg, W. E. *Isr. J. Chem.* **1977**, *15*, 311–317.
(47) Stanford, M. A.; Swarty, J. C.; Phillips, T. E.; Hoffman, B. M. *J. Am. Chem. Soc.* **1980**, *102*, 4492–4499.
(48) Valentine, J. S.; Sheridan, R. P.; Allen, L. C.; Kahn, P. C. *Proc. Natl. Acad. Sci. U.S.A.* **1979**, *76*, 1009–1013.
(49) Friedman, J. M.; Rousseau, D. L.; Ondrais, M. R. *Annu. Rev. Phys. Chem.* **1982**, *33*, 471.

Mb (ref 4, this work); (5) weak (or vanishing) coupling of the Fe–N_{His} mode in oxy Hb, Mb (no Fe–N_{His} mode has been definitively assigned in *any* ligated complex) (ref 6 and 40); and (6) no change in the Fe–O_2 stretching frequency (or other Fe–ligand frequencies) between R and T forms of Hb (ref 3 and 40).

While the above models have certain attractive features, we are not convinced that they contain all of the necessary ingredients needed to integrate all of the recent Raman observations into a consistent picture. For example, our observations of strong Fe–N_{His} coupling to the Soret resonance are not easily explained. We are skeptical that coupling of the observed magnitude can proceed via an indirect route involving the $d\pi$ orbitals of the iron atom, since the histidine π-electrons are not significantly involved in binding to the iron (i.e., the Fe–N_{His} bond is primarily σ in character). Non-bonding repulsive interactions are also unlikely candidates for the coupling since the REP follows the assumed harmonic potential energy surface so well. In addition, observations 4 and 5 above are inconsistent with non-bonded coupling, since we would expect to see stronger T-state coupling as well as Fe–N_{His} scattering from the ligated systems.

As a result of these difficulties we have explored an alternative coupling hypothesis that explains quite simply the Raman observations 1–6. So far as we can determine, this hypothesis appears to be consistent with existing X-ray data and model compound studies.

The hypothesis rests on the lowered symmetry of the heme group in Hb and Mb. The fact that the Fe–N_{His} bond is tilted with respect to the heme plane in the deoxy species and that the iron atom is out of plane (ca. 0.5 Å) means that the 3d orbitals of the iron atom are mixed. Furthermore, the sp^2 lone-pair orbital from histidine will interact with the "dz^2" iron orbital along a line that is not perpendicular to the heme plane. We denote the orientation of this bond in Figure 12C. High-resolution X-ray studies[50-52] indicate that the polar angle, θ, is on the order of 10° in the deoxy structures and decreases to ca. 0° upon ligand binding. In addition, the azimuthal angle, ϕ, is on the order of 15–25° in the deoxy structures and also decreases to small values (i.e., the histidine plane eclipses the N_1–N_3 axis) in the ligated form. The key question that has not yet been answered by the X-ray data is the following: what are the local structural changes that take place at the *deoxy* heme site following the T → R quaternary transformation?

In the present analysis we consider changes in the azimuthal angle, ϕ, to be of significant importance and argue that a decrease of ϕ (at the *deoxy* heme site) following the T → R transformation can lead directly to observations 1–6 as well as the observed red shift[44] of the Soret band. It is possible that these same interactions contribute to the energetics of cooperativity (i.e., $\Delta G = \Delta G_R - \Delta G_T \simeq 3.4$ kcal/mol).

A hidden assumption in the current models of cooperativity is that the same decrease in θ will occur at the *deoxy* heme site as is observed for *ligated* Hb in the R quaternary structure. Our view is that the binding of the ligand produces a significant perturbation on the Fe–N_{His} bond angle (θ) and, in fact, the binding process itself may cause at least part of the observed reduction in θ. It seems conceivable that the local structural alterations of the deoxy binding site (following the T → R quaternary changes) involve a decrease in ϕ rather than θ. (We do not exclude the possibility that both angles are reduced, but it is necessary in the present model that θ remain non-zero in the deoxy R structure, see Figure 12B). It is important to note that all of the "high-affinity" deoxy structures so far analyzed (i.e., Mb, α- and β-subunits) do have $\theta \sim 10°$.

In order to understand why the azimuthal angle, ϕ, is so important, it is necessary to recall that there are *three* σ electrons participating in the high-spin ferrous bond between histidine and iron. Two of these are donated from the sp^2 lone-pair hybrid orbital of histidine and reside primarily in the $\sigma_{Fe-N_{His}}$ bonding orbital located between the iron and N_{His} atoms. The third electron comes from the iron atom itself and is located in the antibonding $\sigma^*_{Fe-N_{His}}$ orbital which extends to the distal side of the iron atom along the Fe–N_{His} vector determined by the angles θ and ϕ. Since this orbital is predominantly 3d in character, it is important to note that the radial extent of $\sigma^*_{Fe-N_{His}}$ is significant (ca. 5 Å for 3d hydrogenic orbitals[53]). As the azimuthal angle, ϕ, is reduced in the deoxy R state, the electron density in the $\sigma^*_{Fe-N_{His}}$ orbital will suffer stronger electron–electron repulsion with the filled π-electron orbitals of the porphyrin nitrogen (N_3). Moreover, as depicted in Figure 12D, there can also be significant non-zero overlap between $\sigma^*_{Fe-N_{His}}$ and the π^*_{por} antibonding orbitals of the porphyrin. This overlap will increase as ϕ becomes smaller, and some relief from the repulsion energy may be achieved by mixing and delocalization of electron density from $\sigma^*_{Fe-N_{His}}$ to π^*_{por}. Contributions to the free energy of cooperativity can obviously arise from this type of interaction, see Figure 12B. In addition, such an effect would cause a red shift in the Soret absorption upon the transformation deoxy T → deoxy R. Note also that a distribution in ϕ within a given tertiary structure of Hb and Mb (i.e., conformational substates) would lead to an inhomogeneous broadening of the absorption band as well as a broadening of the 220-cm^{-1} Raman mode (this mode is unusually broad for heme protein Raman spectra).

The six Raman observations also follow directly: (1) strong (harmonic) coupling to the Soret transition due to direct mixing of π^*_{por} and $\sigma^*_{Fe-N_{His}}$; (2) decreased ϕ in the deoxy R state leads to a decrease in the $\sigma^*_{Fe-N_{His}}$ electron density and an increase in the Fe–N_{His} mode frequency; (3) the inverse relationship with the ν_4 mode frequency (i.e., decrease in ν_4) follows due to increased π^*_{por} electron density in the deoxy R state; (4) the Fe–N_{His} scattering from the deoxy T state is reduced due to a larger value of ϕ and less mixing and coupling to the π–π^* Soret resonance; (5) no coupling to ligated systems since $\sigma^*_{Fe-N_{His}}$ is involved in mixing and bonding with ligand orbitals; and (6) the present hypothesis involves subtle differences in the *deoxy* R and T structures and does not necessarily imply that significant iron ligand perturbations need be present in the oxy complex (on the other hand, the hypothesis does not exclude such perturbations in the ligated state although, as noted previously,[40,54] they are difficult to reconcile with observation 6).

Clearly, the local structural change described above involves an increase in energy of the deoxy heme system upon the T → R conversion. This local change, which directly influences the oxygen affinity (Figure 12B), must of course be driven by a global reduction in the free energy of the entire Hb molecule. Such a global free energy change may involve a reduction in interaction energy which is distributed throughout the Hb molecule or by the local decrease in energy achieved by the oxygenated hemes when the T → R switch occurs. The net heme localized free energy change is given by $(4 - n)|\Delta G_D| - n|\Delta G_0|$ if n is the number of oxygens bound to the system when the T → R transition takes place. Note that this contribution is highly "cooperative" and favors the transition as more oxygens are bound. An increase in entropy of the system (e.g., breaking of various salt bridges) may also help to drive the overall process.

Although the above hypothesis may seem extreme to some workers in the field, we put it forward in the spirit of objective scientific inquiry. If high-resolution X-ray structures of the *deoxy* R state become available it should be possible to experimentally confirm or reject the above hypothesis. We would predict a decrease in ϕ upon the deoxy T → deoxy R transformation along with a decrease in θ (but not to zero). We might expect the decrease in θ as an additional means by which the electron–electron repulsion between $\sigma^*_{Fe-N_{His}}$ and π_{por} can be reduced. Such interactions may also give rise to forces that aid the bulk F-helix motion.

(50) Takano, T. *J. Mol. Biol.* **1977**, *110*, 569–584.
(51) Phillips, S. E. V. *J. Mol. Biol.* **1980**, *142*, 531–554.
(52) Baldwin, J.; Chothia, C. *J. Mol. Biol.* **1979**, *129*, 175–220.
(53) Leighton, R. B. "Principles of Modern Physics"; McGraw-Hill: New York, 1959; p 176.
(54) Walters, M.; Spiro, T.; Suslick, K.; Collman, J. *J. Am. Chem. Soc.* **1980**, *102*, 6857–6858.

Additional insight may be gained through further Raman studies. It is interesting to note that the $\sigma^*_{Fe-N_{His}} \leftrightarrow \pi^*_{por}$ and $\pi_{His} \leftrightarrow d\pi(Fe) \leftrightarrow \pi^*_{por}$ coupling schemes are orthogonal and will be expressed through different components of the polarizability tensor: α_{xx} and α_{yy}, respectively ($N_1 - N_3$ defines the x axis, Figure 12C). Each mechanism should couple asymmetrically to the x- and y-polarized transition moments and give rise to $\rho = 0.125 - 0.33$ depending on their relative balance. More careful measurements of the polarization properties of the resonant scattering of the $Fe-N_{His}$ mode may help us to clarify this point.

Finally, it should be emphasized that our hypothesis predicts little or no Soret coupling to the $Fe-N_{His}$ mode if $\theta \rightarrow 0$. In fact, this prediction appears to be largely realized in the model compound studies of Hori and Kitagawa.[55] In this Raman investigation of $Fe^{2+}(T_{PivP}PP)$(1-MeIm) and $Fe^{2+}(T_{PivP}PP)$(2-MeIm) and their oxy complexes we see almost no scattering intensity due to the $Fe-N_{His}$ mode in the symmetric ($\theta \simeq 0$) 1-MeIm complex when compared to the asymmetric ($\theta \simeq 10°$) 2-MeIm complex.[56] (However, there is some question as to whether the iron atom in the 1-MeIm complex is actually 5-coordinate as claimed.[55]) This observation suggests that the observed Raman scattering of the 220-cm^{-1} mode in the deoxy R-state Hb and Mb results from the $\theta \neq 0$ condition. If $d\pi(Fe)$ or non-bonding repulsive interactions were responsible, we might expect them to be operative regardless of the value of θ.

It remains to be seen whether the above hypothesis will hold up to further scrutiny. One of the most interesting questions raised so far involves the observation of a strong $Fe-N_{His}$ vibration in the 10-ns photolyzed transient species of R-state Hb.[45] In order for this observation to be consistent with the arguments given above, one must assume that, after photolysis, both the iron and histidine relax rapidly (within picoseconds)[45b] to an out-of-plane configuration with $\theta \neq 0$. Model building suggests that the rapid histidine motion away from the heme plane, parallel to the z axis, may indeed be coupled to a change in polar angle (if the F helix is held fixed, rotation about the methylene carbon-α carbon bond will lead to strong coupling of the z and θ motions). The azimuthal relaxation must then proceed on a much slower time scale and presumably involves coupling to the bulk F-helix motion. In any case, we suggest that the azimuthal parameter, ϕ, must be given important consideration in any local analysis of cooperativity since the steric repulsions that play such an important role in many of the current models must also be affected by this crucial degree of freedom. In fact, it is probably a combination of steric and electron delocalization effects (as modulated by θ, ϕ, and the out-of-plane displacement) that determines the local energetics and the $Fe-N_{His}$ bond strength. Perhaps molecular dynamics simulations can ultimately help us to understand this intriguing problem in more detail.

C. Summary. We have presented the first Raman excitation profiles of the $Fe-N_{His}$ modes of deoxy Mb and deoxy Hb. We have utilized a Kramers-Kronig transform analysis to find that these modes are relatively strongly coupled $S = [0.06 - 0.16]$ to the Soret resonance. The large uncertainty in the value of S arises primarily from a lack of quantitative information about inhomogeneous conformational effects in these systems. Nevertheless, further work on this problem utilizing both the REP (1357-cm^{-1} mode) and absorption band shapes promises to help quantify the magnitude of the conformational broadening.[57] The technique of inverse transformation of REP line shapes has also been presented in order to demonstrate how careful resonance Raman measurements can resolve overlapping and congested electronic absorption spectra. In addition, we have discussed how the opposite phasing of the Condon scattering amplitude leads to discrimination against the observation of low-frequency vibrations. The observed blue shift of the REP of the 150-cm^{-1} feature remains unexplained and could conceivably be attributed to an underlying charge-transfer transition. Careful polarization studies may help to resolve this possibility. Finally, we have presented a new hypothesis that explains the coupling of the $Fe-N_{His}$ mode to the Soret resonance as well as numerous other Raman observations.

Acknowledgment. This work is supported by grants from the National Institute of Health (AM30714), the Research Corporation, and the National Science Foundation (PRM-8213711). One of us (P.M.C.) acknowledges helpful conversations with J. M. Friedman, T. G. Spiro, and K. S. Suslick.

(55) Hori, H.; Kitagawa, T. *J. Am. Chem. Soc.* **1980**, *102*, 3608-3613.
(56) Collman, J. P.; Brauman, J. I.; Rose, E.; Suslick, K. S. *J. Am. Chem. Soc.* **1978**, *100*, 6769-6770.
(57) Bangcharoenpaurpong, O.; Champion, P. M., in preparation.

Calcium-Binding Proteins: Calcium(II)-Lanthanide(III) Exchange in Carp Parvalbumin

Thomas C. Williams,* David C. Corson, and Brian D. Sykes

Contribution from the MRC Group on Protein Structure and Function and the Department of Biochemistry, University of Alberta, Edmonton, Alberta, Canada T6G 2H7.
Received December 23, 1983

Abstract: The CD and EF calcium(II)-binding sites of carp parvalbumin differ not only structurally but also functionally: one domain shows significant selectivity in lanthanide(III) exchange and the other does not. By analyzing the diamagnetically shifted His-26 and N-terminus acetyl ^1H NMR resonances of parvalbumin, we have determined that the selective site is the CD metal-ion-binding domain. The nonselective site is the EF domain. This site-dependent lanthanide selectivity of parvalbumin was further corroborated by determination of its CD- and EF-domain affinities for cerium(III), a paramagnetic lanthanide ion: $K^{CD}_{D,Ce} = 3.2 \times 10^{-11}$ M and $K^{EF}_{D,Ce} = 4.8 \times 10^{-11}$ M. By analogy to the metal-ion-binding properties of cryptands, we conclude that the EF-domain ligands are flexible, expanding or contracting relative to their calcium(II)-coordinating positions in response to lanthanide(III) exchange, whereas the ligand cage provided by the CD domain is rigid.

Parvalbumins are small ($M_r \simeq 12000$), highly acidic proteins noted primarily for their ability to tightly chelate two calcium(II) ions ($K_D \simeq 10^{-9}$ M).[1] X-ray crystallography of carp parvalbumin (isozyme pI 4.25) shows only five oxygen-containing ligands co-

0002-7863/84/1506-5698$01.50/0